PHYSICAL REVIEW B VOLUME 26, NUMBER 3 1 AUGUST 1982

Low-energy electron-loss spectroscopy and Auger-electron-spectroscopy studies of noble-metal—silicon interfaces: Si-Au system

P. Perfetti, S. Nannarone, F. Patella, C. Quaresima, M. Capozi, and A. Savoia
PULS-Gruppo Nazionale di Struttura della Materia-Istituto Nazionale di Física Nucleare, Laboratori Nazionali di Frascati, 00044 Frascati, Italy

G. Ottaviani
Istituo di Fisica, Università di Modena, 41100 Modena, Italy and Gruppo Nazionale di Struttura della Materia-Consiglio Nazionale delle Ricerche, 41100 Modena, Italy

(Received 17 November 1981)

We report complete low-energy electron-loss spectroscopy (LEELS) and Auger-electron-spectroscopy measurements on the Si(111)-(2×1)—Au system at different thicknesses of Au deposited at room temperature and for different annealing cycles. Two overlayer thickness ranges correspond to two different stages of interface formation. In the submonolayer range gold atoms stick on the silicon surface without intermixing and give rise to strong interface LEELS features. A thickness of two monolayers is the lower limit over which intermixing occurs and an Au-Si alloy is formed. The alloy composition changes with overlayer thickness up to 20 ML. Above this value pure gold begins to grow with some silicon outdiffused to the free surface. LEELS data show that in the alloyed phase the shallowest *d* electrons are those mostly involved in bond formation with silicon *sp* electrons. The hybrid bonds correspond to new electronic states at 3.7 eV under E_F for the silicon-rich Au-Si mixed phase.

I. INTRODUCTION

We report a complete set of low-energy electron-loss-spectroscopy (LEELS) and Auger-electron-spectroscopy (AES) measurements on the Si(111)-Au system at different thicknesses of Au deposited at room temperature (RT). Both low [≤ 1 monolayer (ML)] and high Au coverages (up to 100 ML) were explored, and annealing cycles up to 500 °C were performed on samples with different Au thicknesses. This work deals with the question of the interaction of the metal overlayer and the silicon substrate and the subsequent formation of an abrupt or diffuse interface. The existence of interface states as well as intermixed phase electronic states will be examined in detail.

Gold is widely employed in mincroelectronics, e.g., for Ohmic contacts and for Schottky barriers.[1] The Si-Au system has been widely studied in the past. Only recently, however, has a great insight into the physical problems connected to the interface formation been reached with surface-sensitive techniques such as ultraviolet photoemission spectroscopy[2–4] (UPS), AES,[5–8] low-energy electron diffraction[5,8] (LEED), and LEELS.[9–11] The formation of gold silicides with a well-defined stoichiometry does not occur when gold is evaporated on a silicon substrate at RT, while it might occur during the subsequent annealing of this system. When more than 1 ML of gold is deposited at RT, an intermixing between the two materials occurs, and an amorphous or disordered phase is detected by LEED.[8,11] The minimum Au thickness above which interdiffusion occurs is still controversial. The analysis of the UPS core-level emission intensity reported in Ref. 2 would suggest that gold and silicon are mixed together as soon as the gold reaches the surface. In contrast, AES, LEED, LEELS,[11] and ion backscattering studies[13] indicate that interdiffusion occurs above a critical Au thickness ~ 5 ML. Beyond this critical thickness there is a general agreement that an intermixing process takes place. AES depth profiling[5,8] and UPS (Ref. 2) have shown that the intermixed region at the interface is approximately 20 Å thick. For nominal Au coverages thicker than this value the system consists of a sequence of regions: the silicon substrate, an intermixed region (~ 20 Å thick), a pure-gold region, and a very thin (1—2 ML) intermixed phase on top of the pure-gold region. This last phase is due to outdiffusion of Si atoms.

The above qualitative description is valid both for Si(111)-Au (Ref. 5) and Si(100)-Au (Ref. 8) interfaces. The intermixed phase does not show any structural order in LEED. An analysis of the relative intensity of the Au *OVV* and Si *LVV* Auger peaks versus gold coverage (see Sec. III B) indicates that the alloy composition changes from a Si-rich phase near the interface to a Au-rich phase. A different structure is obtained when the above-mentioned Si-Au system is annealed at temperatures of 200–400 °C. An ordered phase has been revealed by LEED with patterns different for gold deposited on Si(111) (Ref. 5) or Si(100) (Ref. 8).

Our present experiments use LEELS and AES to study the Si-Au system obtained by evaporation of Au on RT substrates with or without subsequent annealing. The theoretical framework of LEELS is described in detail in Ref. 14. In summary, within the dielectric theory LEELS results are described by the bulk and surface loss functions ($\mathscr{L}$):

$$\mathscr{L}_{\text{bulk}} \propto -\text{Im}\left[\frac{1}{\tilde{\epsilon}(\omega)}\right], \tag{1}$$

$$\mathscr{L}_{\text{surface}} \propto -\text{Im}\left[\frac{1}{\tilde{\epsilon}(\omega)+1}\right], \tag{2}$$

where $\tilde{\epsilon}(\omega)$ is the complex dielectric function. Owing to the presence of both the real and the imaginary parts of the dielectric function in the $\mathscr{L}$'s, one-electron peaks in the optical absorption spectra do not appear at the same transition energy as the corresponding peaks in LEELS. In Ref. 15 a one-to-one correspondence between peaks of $\epsilon_2(\omega)$ and dips of the second derivative of $\mathscr{L}_{\text{bulk}}$ was established. Since no similar correspondence has yet been established for $\mathscr{L}_{\text{surface}}$ we use in this work the conventional method of analyzing the evolution of peaks rather than dips in the LEELS curves during the interface formation. This problem does not occur for losses involving transition starting from core levels, since for the high-energy-loss region the loss functions are simply proportional to $\epsilon_2(\omega)$. In our analysis we will not try to assign the overlayer-induced LEELS structures to any particular one-electron-like transition. This identification would require optical constants and theoretical band-structure calculations of the corresponding system not available at present. The gold-induced LEELS structures will be used instead to understand the overlayer-substrate interaction, and we shall identify them as to be due either to plasmon losses or to some type of one-electron transitions.

We shall describe the experimental procedure in Sec. II and the experimental results in Sec. III. Section III is divided in three subsections describing LEELS, AES, and scanning electron microscopy (SEM) results. In Sec. IV the results will be discussed for the low coverage range (<1 ML) and for the high coverage range (>1 ML). The conclusions are reported in Sec. V.

II. EXPERIMENTAL PROCEDURES

Clean silicon (111)-(2×1) surfaces were obtained by cleaving an *n*-type silicon bar ($\rho \simeq 0.05\ \Omega$ cm) in an ultrahigh-vacuum chamber at a base pressure of the order of 1×10^{-10} Torr. Notches on the bar allowed many cleaves without breaking the vacuum. Gold was deposited by thermal evaporation from a tungsten crucible. The evaporated film was increased step by step from a fraction of a monolayer to 100 ML. All depositions were done with the silicon substrate at RT, and the annealing cycles (see Sec. III) were performed with a resistive heating system on the back of the sample holder. Great care was used in degassing the tungsten crucible to avoid contamination of the sample. During the depositions the vacuum pressure was always lower than 3×10^{-10} Torr, and no trace of contaminants was in the Auger spectra (sensitivity of 10^{-2} ML of carbon). The film thickness was measured by a piezoelectric monitor. The nominal one-monolayer coverage ($\Theta=1$) was defined as one Au atom per substrate atom [Si(111) surface density $\sim7.8\times10^{14}$ atoms/cm^{-2}], corresponding to a nominal thickness of 1.3 Å. The electron-energy analyzer used was a Physical Electronics double-pass cylindrical mirror (CMA), and its coaxial electron gun was applied both for AES and LEELS spectroscopy. For AES the primary electron-beam energy was 3 keV with a 2-mA emission current and 2-V modulation voltage applied to the analyzer. For LEELS the primary electron-beam energy was lowered down to $\simeq$100 eV, and the angle of incidence was 45° with respect to the sample normal. A phase-sensitive detection system was used in the first- and second-derivative modes. Low-energy electron diffraction patterns were used to check the crystal structure of the clean and Au-covered silicon surfaces. The results reported here, taken at RT, correspond to several different sequences and/or annealing cycles. After some of these runs the surface morphology was investigated by SEM.

III. RESULTS

A. Low-energy electron-loss results

Figure 1 gives a summary of a different series of LEELS measurements. Each run corresponds to one of the solid lines and to the reference number on it. Each run consists of successive Au depositions followed by annealing. The annealing temperature and the coverage step were changed from run to run, while the annealing time was 30 min. For each annealing step, $\times$'s on the solid lines show the stage of each run at which LEELS, AES, and LEED were performed.

LEELS curves for run 1 are reported in Fig. 2. The left-hand side of the figure shows the evolution of the spectrum for increasing Au coverage in the submonolayer region. The right-hand side of this figure shows the effects of the annealing. The first left-hand side spectrum corresponds to clean Si(111), and all features have been previously identified. In particular, the peaks at 16.9 and 11.0 eV correspond to bulk- and surface-plasmon losses. Peaks E_1 at 3.6 eV and E_2 at 5.2 eV are one-electron transitions related to the bulk-Si band structure. The remaining losses S_1, S_2, and S_3 at 2.4, 6.9, and 15.1 eV involve transitions between back-bond surface states and empty surface states. A small amount of gold causes a strong modification of the spectrum. The surface losses disappear at 0.4-ML coverage. A new structure I_{S_2} appears at 7.6 eV for a 0.2-ML coverage. Its position shifts to 7.0 eV at 0.6 ML and does not change for higher coverages. We interpret the structure I_{S_1} at 2.2 eV as a gold-induced feature rather than a surviving S_1 peak since the S_1 transition that involves the Si dangling bonds is removed by a very small amount of deposited materials.[16] As we shall see later, peaks $I_{S_1}, I_{S_2}, I_{S_3}, I_{S_4}$ are observed at low coverages and disappear at higher coverages; therefore we interpret them as interface features. An interesting result shown on the right-hand side of Fig. 2 is that each 30-min annealing step does not change the peak positions up to 500 °C. The most striking effect of temperature is the narrowing of all spectral features. The above-mentioned results are summarized in Fig. 3, where the energy of the LEELS features is shown as a function of coverage and annealing temperature. The sharp (2×1) LEED pattern of the Si(111) cleaved face becomes weak at 1-ML coverage and completely disappears at higher coverages.

In Fig. 4 we report the results of run 3. Here the Au coverage was increased by large increments to follow the evolution of spectra until the pure Au-like situation is reached at 100 ML. Note that the energy resolution was slightly worse here than for the other runs. The broad low-energy peak at $\Theta=2$ corresponds to the double peak at $\Theta=5$. The evolution saturates at $\Theta=12-30$ when all new structures B,C,D,E,F are well developed. Peak B is already well defined for $\Theta=5$, and its energy position is 3.7 eV. For higher coverages it shifts to lower energy and reaches its final posi-

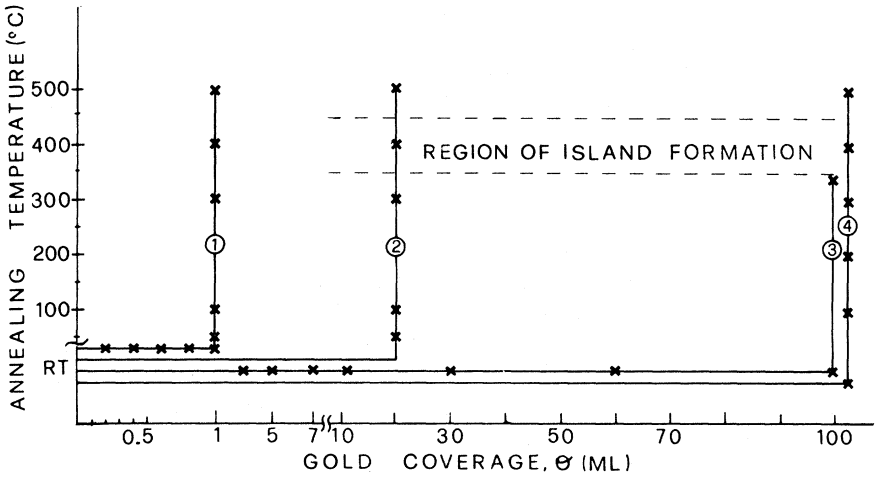

FIG. 1. Each line corresponds to a different run identified by the reference number on the line. Each run consists of successive depositions at RT followed by annealing. The region where island formation occurs is indicated by dashed lines.

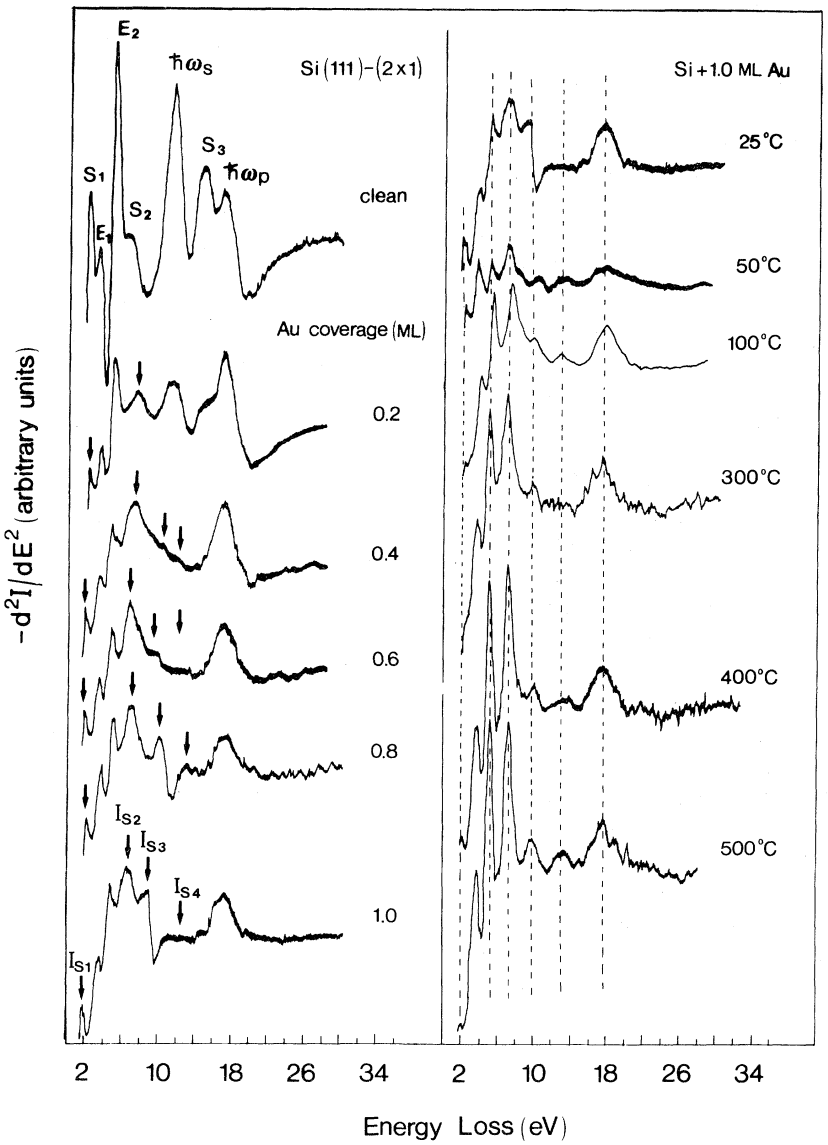

FIG. 2. LEELS curves of clean cleaved Si(111)-(2×1) and of the same surfaces covered with different thicknesses of gold (submonolayer coverage). The right-hand side of the figure shows the spectra obtained after 30 min of annealing at different temperatures for 1-ML coverage.

tion, 2.5 eV, around $\Theta=30$. The other structures *C,D,E,F* at 6, 11, 16, and 22 eV remain unchanged above $\Theta=12$. Figure 5 shows the energy position of peak *B* as a function of Au coverage. The observed shift cannot be attributed to a background effect. In fact, the same effect should otherwise be seen also for peak *C*.

We have seen in Fig. 2 that 1 ML of gold forms a stable system—no changes in the LEELS spectrum are caused by the annealing processes. We will show now that this stability depends on the gold thickness. The effects of the annealing cycles for a 20-ML-thick Au overlayer are reported in Fig. 6. In the RT spectrum peak *C* now seems to be a convolution of two different peaks. Peaks *E* and *F* are less evident in Fig. 6 than in Fig. 4. The effects of annealing are dramatic in Fig. 6, and the spectrum is completely changed at the end of the annealing cycle. The peak evolution is more evident from Fig. 7. After 100 °C peaks *C* and *D* are well split and evolve into four structures at 5.4, 7.0, 10.6, and 13.0 eV. Peak *B* rises slightly in energy, and at 400 °C it has the same energy as peak E_1 in the clean silicon. The bulk-silicon plasmon

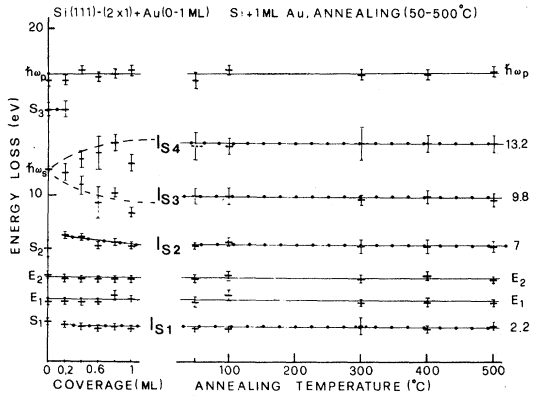

FIG. 3. Energy positions of LEELS features vs Au coverage and annealing temperature. Dots on solid lines indicate surface and interface losses. Dashed lines are the best fit of Eq. (6) to the experimental results (see text).

reappears at 400 °C, and all structures at 500 °C correspond to those seen for the $\Theta=1$ spectrum, Fig. 2. Similar results are shown for run 4 in Figs. 8 and 9. Here the annealing process again splits both peaks *D* and *C* and the 500 °C annealing step reestablishes the $\Theta=1$ spectrum. The major difference between run 2 and run 4 is that the splitting of peaks *D* and *C* occurs at higher temperatures for the latter run.

B. Auger-spectroscopy results

The Auger processes involving the valence band yield information about the local density of states of the ionized atom if the Coulomb interaction between the two holes is small compared to the bandwidth.[17–19] This is the case of the Si *LVV* Auger transition. Therefore the single peak observed at 92 eV (see Fig. 10) is interpreted as a self-convolution of the partial *sp* density of states. Therefore the modifications of the Si *LVV* line shape observed in Fig. 10 probe the involvement of Si *p*-like states in the substrate-overlayer chemical bond. One monolayer of Au gives a Au *OVV* peak at 69 eV, and in the submonolayer range it affects only the intensity of the silicon peak. At $\Theta=5$ the gold structure becomes dominant, and the Si *LVV* feature splits into two peaks at 90 and 95 eV. This spectrum does not change for larger coverages except for the relative intensity of its two components. A striking effect is the persistence in the spectrum of the Si doublet up to at least $\Theta=100$. The intensity ratio $I_{\mathrm{Au}\,OVV}/I_{\mathrm{Si}\,LVV}$ is shown in Fig. 11 as a function of Θ. The ratio exhibits a continuous increase, which saturates at $\Theta \gtrsim 20$. In the inset of Fig. 11 the intensity ratio versus Θ plot is shown in detail for the submonolayer region. A linear behavior is observed for $\Theta \lesssim 1$. The evolution of the low-energy Auger spectrum for $\Theta=20$ is shown in Fig. 12 as a function of annealing. The double silicon peak characteristic of $\Theta=20$ undergoes a strong change and it reaches its final single-peak line shape between 400 and 500 °C. Similar results were obtained for $\Theta=100$ after the same annealing cycle. The intensity ratio between the Si *KLL* and the Au *MNN* Auger peaks for the annealing cycles of the 20- and 100-ML coverages are shown in Fig. 13 together with $I_{\mathrm{Au}\,OVV}/I_{\mathrm{Si}\,LVV}$ of $\Theta=1$. The study of the high-energy Auger lines is complementary to that of lines involving the valence band. In fact, intermixing processes between gold and silicon strongly influence the valence-band states, while they weakly affect the core levels. Therefore the interpretation of the spectra becomes simpler in the latter case.

C. Surface morphology

The surface morphology was investigated with a scanning electron microscope. The analysis was performed mainly on samples covered with 100 ML of gold. In the as-deposited samples, no particular features are observed, and the gold film appears quite continuous. After annealing at temperatures higher than 350–400 °C gold islands are formed, as shown in Fig. 14. The islands are different in shape with an average height of 1 μm and a bottom area of the order of few μm^2. The percentage of the area covered by the islands is 10% of the total sample area. In Fig. 14 is shown a sketch showing islands connected with a thin gold film. The presence of such a thin film cannot be proved by SEM but only inferred from AES and LEELS results, previously presented. The composition of the islands has been studied with x-ray diffraction technique and is substantially gold dissolved with a slight percentage of silicon at the most. No evidence for compounds has been found.

IV. DISCUSSION

A. Low Au coverages ($\Theta \lesssim 1$)

The results reported in Sec. III for the low coverage range (see Fig. 2) clearly show that a small

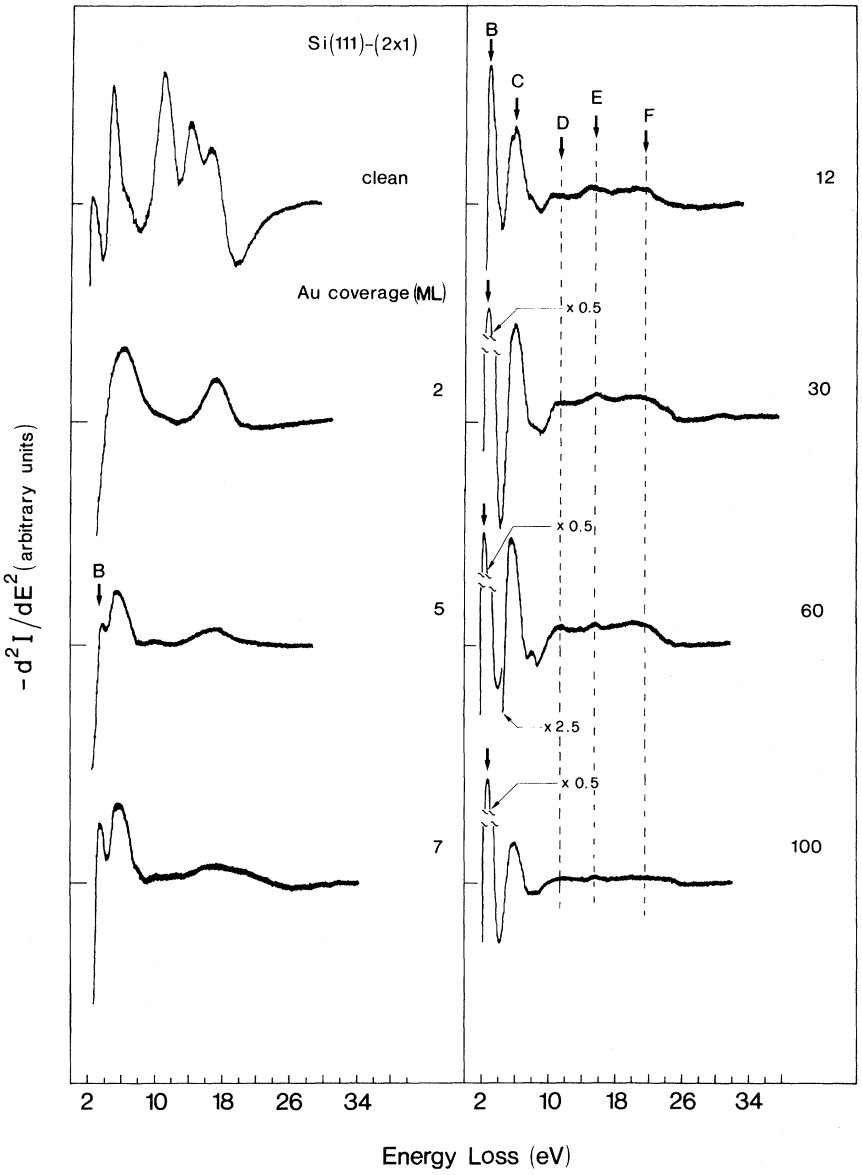

FIG. 4. LEELS curves for clean cleaved Si(111)-(2×1) and for the same surface covered with different Au thickness. The Au coverage is increased by large increments up to $\Theta=100$.

quantity of gold causes a strong change in the LEELS silicon spectrum. The early appearance of the new structures $I_{S_1}-I_{S_4}$ demonstrates that a reaction between silicon and gold occurs. The nature and strength of this reaction require, however, some further analysis. For example, they could be limited to the formation of the Au–Si bond at an abrupt interface or they could correspond to an intermixing between the two atomic species. This analysis will be based in particular on the behavior of the Auger $I_{\mathrm{Au}}/I_{\mathrm{Si}}$ intensity ratio versus gold coverage (Fig. 11) and on the effects of the annealing cycle for $\Theta=1$ (Fig. 2). We observed in Sec. III B that the Si LVV line shape is not affected by gold deposition in the submonolayer region—only a decrease in intensity is detected. If we use the equations

$$I_{\mathrm{Si}}=I_{\mathrm{Si}}^{(0)}e^{-d/L}\,, \tag{3}$$

$$I_{\mathrm{Au}}=I_{\mathrm{Au}}^{\infty}(1-e^{-d/L}) \tag{4}$$

for the Si and Au AES intensities versus d, the

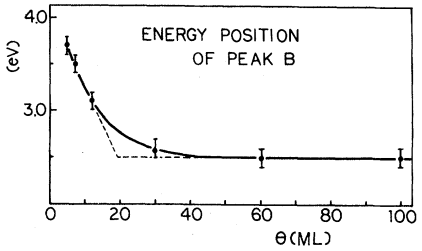

FIG. 5. Energy position of peak B vs the Au coverage.

nominal Au thickness, we obtain

$$\ln\left[\frac{I_{\mathrm{Au}}}{I_{\mathrm{Si}}}+C\right]=\frac{d}{L}+\ln C\ , \tag{5}$$

where $I_{\mathrm{Si}}^{(0)}$ and $I_{\mathrm{Au}}^{(\infty)}$ are the AES intensities of the cleaved silicon and bulk gold, and $C=I_{\mathrm{Au}}^{(\infty)}/I_{\mathrm{Si}}^{(0)}$. The same escape depth L has been used for both materials. This is reasonable since the Si LVV and Au OVV Auger lines have nearly the same energy. In Fig. 15 a plot of $\ln(I_{\mathrm{Au}}/I_{\mathrm{Si}}+C)$ is shown. We used $C=0.92$, calculated from the Auger data reported in Ref. 20. Small changes of C do not affect appreciably the results that follow. The plot of Fig. 15 exhibits a linear behavior, and from its slope we find $L=3.7\pm0.8$. The 0.8-Å uncertainty in L is due essentially to the difficulty in evaluating the Au Auger amplitude at small coverages and to an uncertainty of 10% in the Au thickness. For comparison, the escape depth of Au at a kinetic energy of 70 eV is $\simeq$4 Å (Ref. 21) and that of silicon is $\simeq$5 Å (Ref. 22) at nearly the same kinetic energy. The uncertainty in L does not enable us to evaluate an intermixing between Au and Si atoms less than 5%. Within this limit we can state that at $\Theta\leq 1$ we have a Au uniform growth and an abrupt junction occurs between gold and silicon (see also Ref. 11). In fact, a much higher value of

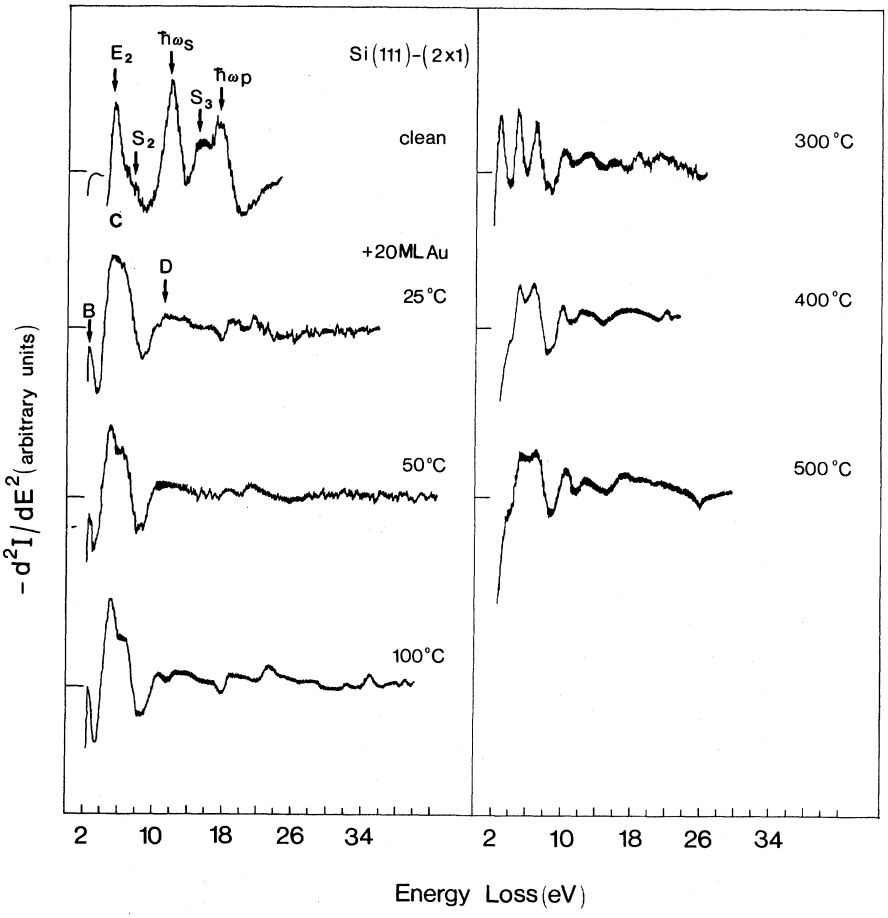

FIG. 6. LEELS spectra for $\Theta=20$ at RT and after different 30-min annealing steps at different temperatures. The top left spectrum is that of clean cleaved Si(111)-(2×1).

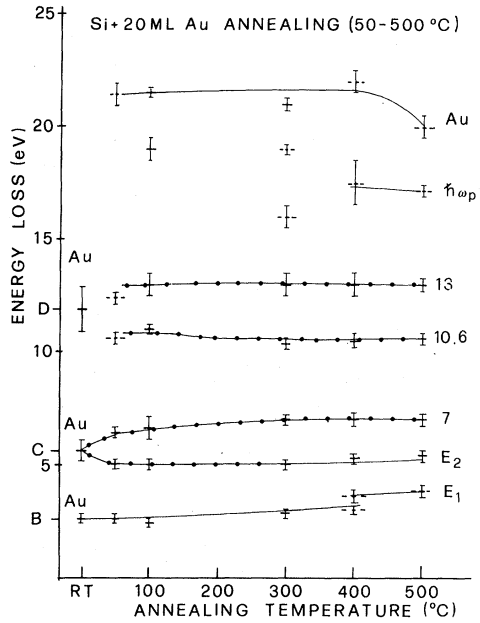

FIG. 7. Energy position of LEELS features for $\Theta=20$ after different annealing steps at different temperatures. Dots on solid lines indicate interface losses. The feature around 5 eV becomes degenerate with the Si bulk loss E_2 and cannot be unambiguously interpreted as an interface loss nor as a Si bulk loss.

L should be obtained from Eq. (3) in the case of strong intermixing or island formation. Note that the exponential behavior of Eqs. (3) and (4) is still a good approximation in the submonolayer region. In fact for $d\rightarrow 0$

$$I_{\mathrm{Au}}/I_{\mathrm{Si}}\simeq Cd/L\ , \tag{6}$$

i.e., a linear behavior. A best fit of Eq. (6) to the experimental results (inset of Fig. 11) gives $L=3.5$ Å. This value coincides within the experimental uncertainty with the value $L=3.7$ Å given above. The hypothesis that at very low coverages no intermixing occurs is independently confirmed by the stability of the interface with temperature. Figure 2 shows that an annealing cycle up to 500 °C does not change the peak positions in the LEELS spectrum. Large changes are seen instead for the higher coverages (see Figs. 6 and 8). One should observe that this interface has a heat of reaction[23,24] $\Delta H_R=0$ (ΔH_R is the difference in heat of formation between bulk silicon and the Si-Au complex). High negative values of ΔH_R correspond to strong reactivity between semiconductor and metal. In Ref. 23, for example, a link has been reported between the interface width and ΔH_R. Stronger reactivity, i.e., larger negative ΔH_R's corresponds to thinner interfaces. In our case it seems that gold shows a different behavior at very small coverages ($\Theta\leq 1$ ML). Its strong reactivity is confirmed by Auger analysis and by the appearance of new LEELS features (Fig. 2) that are not due to the bulk semiconductor nor to the bulk metal.[25]

Similar conclusions were reached in Refs. 11, 12, and 13 on the basis of Auger analysis, electron microscope observations, and ion backscattering experiments. In Ref. 11 a critical Au thickness limit (~ 5 Å) was reported above which the interdiffusion begins. Silicon disruption is explained there as due to the screening by metal electrons of the Coulomb interaction between silicon atoms—for a metal-like behavior the Au overlayer should have a thickness above 5—10 ML. This explanation, however, fails for the Si-Ag interfaces where no intermixing occurs at any Ag coverage at RT.[26] Its validity for Si-Au is therefore questionable since these two interfaces should have similar properties. The Si-bond disruption is better explained by the formation of bonds involving Si sp and Au sd electrons. We shall see later that the Si sp—Au sd hybrid bonds in the Au-Si alloy phase are deep enough in the valence band to explain a preferential formation of Au—Si bonds. It remains to be explained why this mechanism starts after a certain Au thickness limit. From our experiments we cannot establish exactly what this limit is. Since at $\Theta=2$ we begin to see changes in the Si LVV Auger line shape, we estimate the limit to be approximatively 2 ML.

The loss peaks like those of Fig. 2 (peaks I_{S_1} through I_{S_4}) could be due, in general, either to single-particle excitations or to localized plasmons. In the latter case the three media, silicon, gold, and vacuum, can be described by the following dielectric functions[27]:

$$\epsilon_{\mathrm{Si}}(\omega)=1+\frac{\omega_{p\,\mathrm{Si}}^2}{\Delta^2-\omega^2}\ ,\quad \epsilon_{\mathrm{Au}}(\omega)=1-\frac{\omega_{p\,\mathrm{Au}}^2}{\omega^2}\ ,$$

$$\epsilon_v=1\ ,$$

where $\hbar\omega_{p\,\mathrm{Si}}=17$ eV and $\hbar\omega_{p\,\mathrm{Au}}=9$ eV are the bulk-plasmon frequencies and Δ accounts for the deviation from the free-electron gas behavior. We are making the hypothesis that gold atoms do not interdiffuse up to 1—2 ML and that the dielectric constant of the metallic film is still that of bulk gold. Using $\epsilon_{\mathrm{Si}}(0)=12$ we find $\Delta^2=26.3$, and the interface-plasmon frequencies can be calculated from the relationships[27–29] $\epsilon_{\mathrm{Si}}=-\epsilon_{\mathrm{Au}}$ and

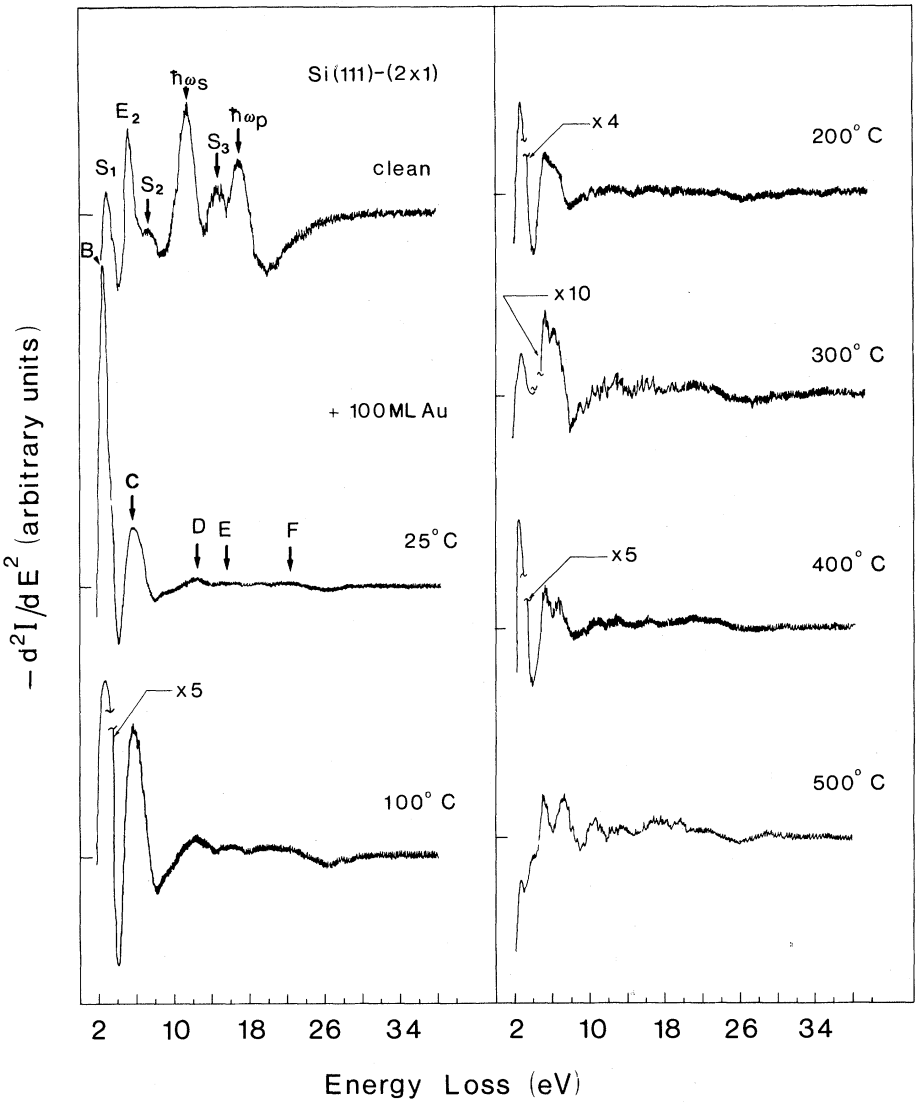

FIG. 8. LEELS spectra for $\Theta=100$ at RT and after different 30-min annealing steps at different temperatures. The top left spectrum correspond to the clean cleaved Si(111)-(2×1).

$\epsilon_{Au}=-1$. The three solutions are 2.3, 14.3, and 6.4 eV, respectively. Only the first of these solutions is close to an experimental loss peak, i.e., I_{S_1} peak. This indicates that mostly one-electron transitions are responsible for the new LEELS features. On the other hand, the detailed nature of these transitions cannot be determined without band-structure calculations.

Note that in Figs. 2 and 3 the losses I_{S_3} and I_{S_4} result from an increasing splitting of the surface-plasmon peak with increasing Au coverage. This splitting can be explained by a simple model calculation[30] in the framework of the dielectric scattering theory under the assumption that the localized gold—silicon bonds give rise to a LEELS feature nearly degenerate in energy with the surface-plasmon loss. In the energy region of interest the silicon dielectric function can be approximated by $\epsilon_{Si}(\omega)=1-\omega_p^2/\omega^2$, where $\hbar\omega_p=17$ eV, and the gold-induced transition can be described by $\epsilon_{Au,i}=A\omega_{Au,i}^2\Theta/(\omega_{Au,i}^2-\omega^2-i\omega\Gamma)$, where A, $\omega_{Au,i}$, Θ, and Γ are the oscillator strength parameter, gold-induced transition frequency, Au coverage, and broadening parameter. Here we used a coverage-dependent oscillator strength under the reasonable assumption that increasing Θ would

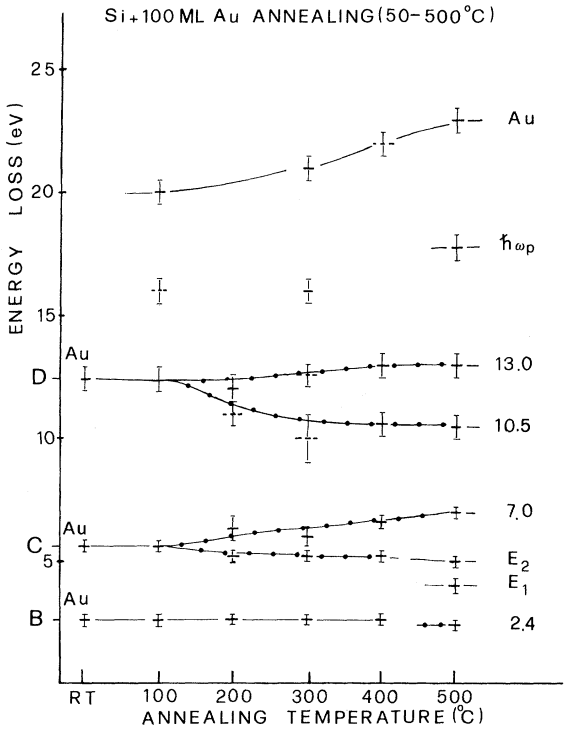

FIG. 9. Energy positions of LEELS features for $\Theta=100$ after different annealing steps at different temperatures. The dots have the same meaning as in Fig. 7.

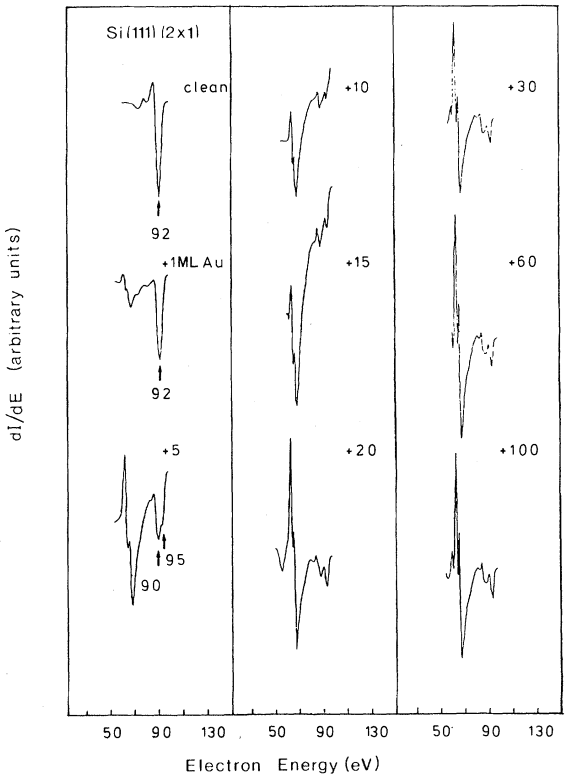

FIG. 10. Low-energy Auger spectra of clean cleaved Si(111)-(2×1) and of the same surface covered with different Au thicknesses.

also proportionally increase the oscillator strength of gold-related transitions. The right-hand side of Eq. (2) now becomes

$$-\mathrm{Im}\left[1\Big/\left[2-\frac{\omega_p^2}{\omega^2}+\frac{A\omega_{\mathrm{Au},i}^2\Theta}{\omega_{\mathrm{Au},i}^2-\omega^2-i\omega\Gamma}\right]\right],$$

and in the simple case of $\Gamma=0$ the $\mathscr{L}_{\mathrm{surface}}$ has maxima when

$$2-\frac{\omega_p^2}{\omega^2}+\frac{A\omega_{\mathrm{Au},i}^2\Theta}{\omega_{\mathrm{Au},i}^2-\omega^2}=0\ . \tag{7}$$

A best fit of Eq. (7) to the experimental results gives the two solutions reported as dashed lines in Fig. 3 with $A=0.3$ and $\hbar\omega_{\mathrm{Au},i}=11$ eV.

B. High Au coverages ($\Theta>1$)

A new physical situation can be inferred by the evolution of LEELS spectra for $\Theta>1$, Sec. III A. Here, more new structures are appearing (see Fig. 4), the origin of which is completely different from that of the submonolayer features. Peak *B* appearing at $\Theta=5$ in Fig. 4 grows simultaneously to the splitting of the Si *LVV* Auger peak shown in Fig. 10. The existence of this silicon doublet indicates that silicon atoms are forming new bonds with gold atoms. The difference with the submonolayer case is that there the new structures coexist with the bulk-silicon LEELS features, while at $\Theta>1$ the spectral features are characteristic of a completely new compound with no bulk-Si contributions. The

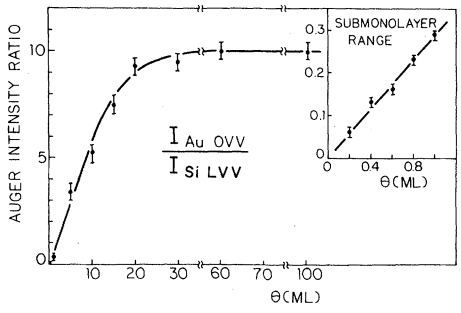

FIG. 11. $I_{\mathrm{Au}\ OVV}/I_{\mathrm{Si}\ LVV}$ Auger intensity vs Θ. The submonolayer range of this plot is shown in the inset. The solid line in the inset is the best fit of Eq. (6) to the experimental results.

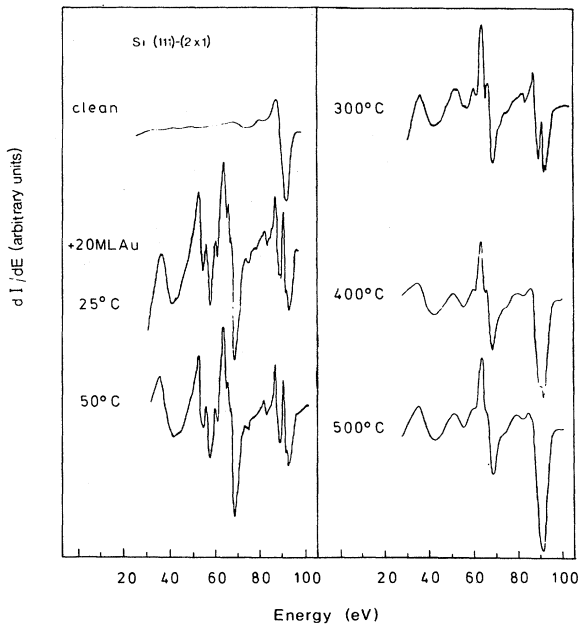

FIG. 12. Low-energy Auger spectrum at $\Theta=20$ and after annealing steps at different temperatures. The top left spectrum corresponds to the clean cleaved Si(111)-(2×1).

splitting of the Si *LVV* Auger line has been reported for similarly prepared systems[5–11] as well as for a Si-Au alloy formed by quenching.[31] We conclude that for $\Theta=5$ an intermixing has occurred between silicon and gold. Peak *B* in Fig. 4 is the only feature that changes in energy for increasing

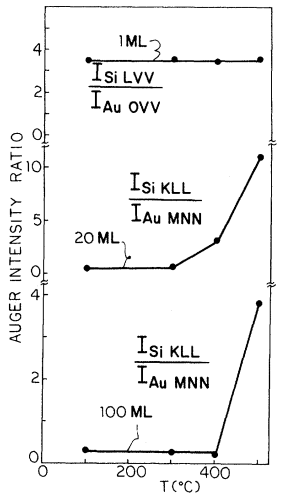

FIG. 13. Auger line intensity ratio, $I_{Si\ KLL}/I_{Au\ MNN}$, for $\Theta=20$ and 100 and $I_{Si\ LVV}/I_{Au\ OVV}$ for $\Theta=1$ vs annealing temperature.

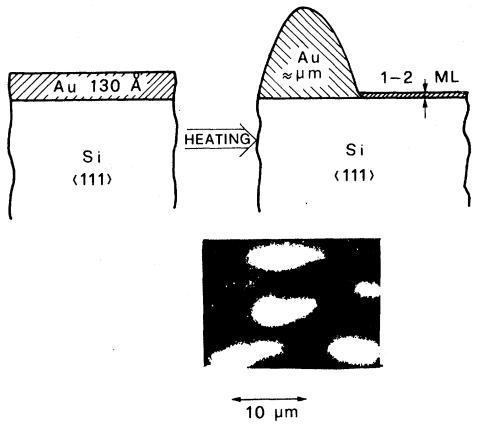

FIG. 14. SEM picture of a sample with 100 ML of gold annealed at 400 °C for 30 min.

Au thickness. Its energy dependence is explained by a dilution of the silicon-atom concentration in the Au-Si alloy for increasing Θ. This dilution is inferred from the behavior of the $I_{Au\ OVV}/I_{Si\ LVV}$ Auger intensity ratio, Fig. 11. A similar shift was observed[32] in the onset of interband transitions in $\epsilon_2(\omega)$ for amorphous gold-silicon alloys of different compositions. If we locate the onset of the interband transitions at the energy for which the $\epsilon_2(\omega)$ behavior deviates from that of the Drude equation (see Figs. 1 and 2 of Ref. 32) we obtain a shift from 3.5 eV for $Au_{0.75}Si_{0.25}$ to 2 eV for a nearly pure gold. The onset of interband absorption in both liquid[33] and solid[34] gold is associated with transitions from the upper *d* band to the Fermi level. The shift of the onset of interband transitions in the Au-Si alloys toward that of pure gold indicates that the shallowest *d* electrons are those

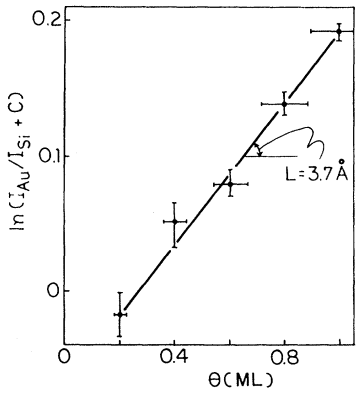

FIG. 15. Plot of $\ln(I_{Au}/I_{Si}+C)$ vs Θ. The slope of the straight line gives an escape depth $L=3.7$ Å.

primarily involved in the bond formation with Si *sp* electrons. This conclusion is confirmed by the shift of peak *B* towards its pure-gold position, 2.5 eV, and by its changing in energy for increasing Θ's (see Fig. 4), while all other features remain unchanged. These results are in agreement with the outcome of the theoretical calculations performed by Bisi and Calandra[35] for the cubic δ-phase Au_3Si, which under certain conditions has been found in thin-film deposition after thermal treatment.[7] According to their conclusions, the *d* states, which in the pure metal lie around 2 eV below E_F, are moved to higher binding energy by hybridization with Si *sp* states, so that the *d* band in the silicide is located between 3.5 and 8 eV below E_F. Only minor *d*-electron structures are found in the density of states between E_F and -3 eV. This indicates that electronic transitions involving *d* states as initial states are expected to shift to lower energies upon increasing metal content in the silicides, as a consequence of increased interaction between *d* states and of the minor role played by the Si $p-$Au *d* hybrides. This trend can be related to the shift of peak *B* in our results (see Fig. 4) for increasing gold content in the Au-Si alloy. Similar theoretical conclusions confirmed by UPS and Auger measurements were found by Ho *et al.*[36] for the Pd-Si system. We emphasize that the overall features of the chemical bonds for Pd_2Si compound are quite similar to those for the amorphous $Pd_{81}Si_{19}$ metallic glass.[37] This confirms the validity of our present approach using theoretical results for single-crystal silicides to interpret experimental results for Si-Au alloys. A correlation can be assumed to exist between the energy position of peak *B* at different Θ and those of the onset of interband transitions measured by optical experiments for different x composition of the $Au_{1-x}Si_x$ amorphous alloy.[32] Using this correlation, we find that the first measurable energy position of *B*, 3.7 eV, corresponds to $x=0.25$, i.e., to a composition $Au_{0.75}Si_{0.25}$ close to the eutectic $Au_{0.81}Si_{0.19}$ composition. This result confirms the hypothesis by Ottaviani *et al.*[38] that the eutectic composition plays an important role in the early stage of formation of metal-semiconductor interfaces. The energy shifts of peak *B* shown in Fig. 5 indicate that the alloy composition varies with Au thickness, reaching a saturation value at $\Theta\approx 20$. This value gives an estimate of the alloy-phase thickness, which agrees with the results obtained by UPS (Ref. 2) and by Auger depth profiling.[5–8] Above $\Theta=20$ the observed LEELS spectra become Au-like even though the low-energy Auger spectra (Fig. 10) show the silicon doublet up to 100 ML. The saturation of the $I_{\mathrm{Au}\,OVV}/I_{\mathrm{Si}\,LVV}$ Auger intensity ratio (Fig. 11) above $\Theta\approx 20$ indicates that the silicon doublet observed up to $\Theta=100$ is due to a second silicon-gold mixed phase at the outer surface. The thickness of this phase has been evaluated by Auger depth profiling[5–8] to be of the order of 1–2 ML. It does not affect, however, the Au-like LEELS spectrum obtained for $\Theta=100$. In fact, all structures $B-F$ may be explained by pure-gold loss-function features calculated by the Kramers-Kronig transform of the optical reflectivity data.[39] For comparison, in Fig. 16 both $-\mathrm{Im}[1/\epsilon(E)]$ and $-\mathrm{Im}[1/\epsilon(E)+1]$ for pure gold are reported together with the measured LEELS spectrum relative to $\Theta=30$.

We have seen in Sec. III that the effects of annealing are completely different for different Au-overlayer thicknesses. In particular, we observed a strong difference between the 1-ML coverage and higher coverages. For $\Theta=1$ the LEELS spectrum does not change with annealing. The Auger intensity ratio $I_{\mathrm{Si}\,LVV}/I_{\mathrm{Au}\,OVV}$ (Fig. 13) also remains constant. We already emphasized that this result provides evidence for a stable electronic and structural configuration at $\Theta=1$ coverage. In contrast, the annealing cycles for $\Theta=20$ and 100 completely reestablish the $\Theta=1$ LEELS spectrum. The spectra corresponding to the last step of each annealing cycle are reported in Fig. 17. The explanation for this similarity is that for high coverages the annealing process creates Au islands. The regions between islands are large in size and give the main

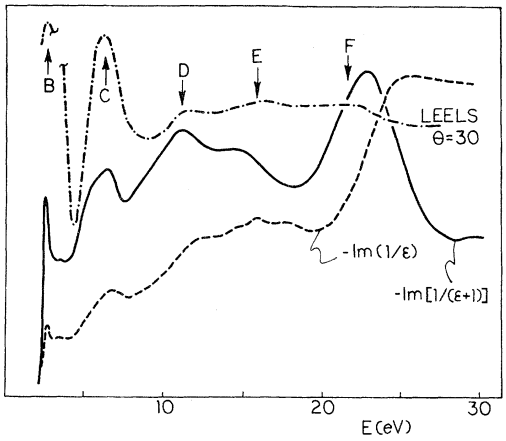

FIG. 16. Comparison of LEELS spectrum obtained at $\Theta=30$ with the bulk and surface loss functions of pure gold.

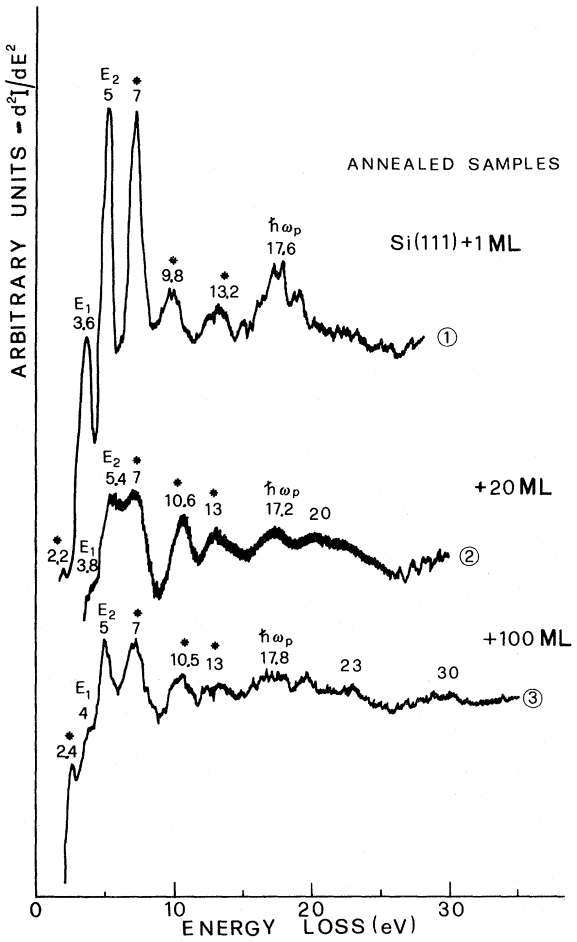

FIG. 17. LEELS spectra obtained after the last annealing step for three different Au coverages: 1, 20, and 100 ML. Stars indicate interface losses.

contributions to the LEELS spectra. The structure and the electronic properties of the regions between islands are similar to those of Si covered by 1 ML of gold. The islands have been detected for $\Theta=100$ by SEM analysis, as reported in Fig. 14. The steep rise of the $I_{\mathrm{Si}\,KLL}/I_{\mathrm{Au}\,MNN}$ Auger intensity ratio between $T=350$ and 450 °C reported in Fig. 13 for $\Theta=20$ and 100 gives an indication of the temperature range in which the islands begin to grow. In the Au-Si phase diagram[40] the equilibrium phase is formed by the separated phases of pure silicon and gold. Thus the temperature effect on island formation is due to the transition from a nonequilibrium mixed phase to the eqiulibrium phase. This conclusion is also evident from the low-energy Auger line shape shown in Fig. 12. Indeed, in the same temperature range the silicon doublet again becomes a single silicon peak coexisting with the gold peak. Island formation was reported by Otter *et al.*[12] on 30-Å annealed Au films deposited on Si(111) and more recently by Tromp *et al.*[41] on the Si-Pd system.

V. CONCLUSIONS

The behavior of RT evaporated Au overlayers on Si is different for two different thickness ranges. In the submonolayer range the chemical reaction between silicon and gold atoms is strong and interface features in LEELS spectra coexist with the clean silicon structures. The persistence of all features at the same energy loss after an annealing cycle up to 500 °C together with the behavior of the $I_{\mathrm{Au}\,OVV}/I_{\mathrm{Si}\,LVV}$ Auger intensity ratio indicate that the system is extremely stable and that gold does not interdiffuse with silicon at low coverage. Interface losses are interpreted as one-electron transitions. At higher coverages the splitting of Si LVV Auger peak shows that the Si–Au bond formation affects the silicon valence-band states. The new situation corresponds to the formation of a Si-Au alloy phase. We have shown that this phase has not a unique composition but it becomes increasingly Au-rich at larger coverages. The thickness of the alloyed phase was estimated to be ~20 ML. Beyond this thickness essentially pure gold is deposited. The effect of annealing for high coverages shows large differences with respect to 1 ML. The LEELS spectrum changes completely, and at the end of each annealing cycle all features of the $\Theta=1$ spectrum are recovered. The evolution of the low-energy Auger peaks and of their intensity versus annealing temperature and a SEM analysis indicate that the annealing causes island formation. This temperature effect is a transition from a nonequilibrium phase (alloyed phase) to an equilibrium state consisting of separated gold and silicon phases.

ACKNOWLEDGMENTS

The authors are indebted to Professor C. Calandra for useful discussions and for making the theoretical results on the cubic δ-phase Au_3Si available to them prior to publication. The technical assistance of R. Bolli, M. Brolatti, and the entire staff of the Instituto Nazionale di Fisica Nucleare (INFN)-Laboratori Nazionali di Frascati is highly appreciated.

[1]A. G. Milnes and P. L. Feucht, *Heterojunction and Metal Semiconductor Junctions* (Academic, New York, 1972).
[2]L. Braicovich, C. M. Garner, P. R. Skeath, C. Y. Su, P. W. Chye, I. Lindau, and W. E. Spicer, Phys. Rev. B 20, 5131 (1980).
[3]I. Abbati, L. Braicovich, and A. Franciosi, Solid State Commun. 33, 881 (1980).
[4]I. Abbati, L. Braicovich, and A. Franciosi, Phys. Lett. 80A, 69 (1980).
[5]A. K. Green and E. Bauer, J. Appl. Phys. 47, 1284 (1979).
[6]G. LeLay, M. Manneville, and R. Kern, Surf. Sci. 65, 261 (1977).
[7]T. J. Magee and J. Peng, Phys. Status Solidi A 49, 313 (1978).
[8]K. Oura and T. Hanowa, Surf. Sci. 82, 202 (1979).
[9]P. Perfetti, S. Nannarone, F. Patella, C. Quaresima, A. Sovoia, F. Cerrina, and M. Capozi, Solid State Commun. 35, 151 (1980).
[10]F. Salvan, A. Cros, and J. Derrien, J. Phys. (Paris) 41, L-337 (1980).
[11]K. Okuno, T. Ito, M. Iwami, and A. Hiraki, Solid State Commun. 34, 493 (1980).
[12]F. A. Otter Jr., H. C. Abbink, and O. L. De Lange, Surf. Sci. 27, 273 (1971).
[13]T. Narusava, K. Kinoshita, and W. M. Gibson, in *Proceedings of the International Conference on Solid Surfaces, Cannes, 1980,* edited by D. D. De Gas and M. Costa (Societe Française du Vide, Paris, 1980), Vol. I, p. 673.
[14]H. Reather, *Excitation of Plasmons and Interband Transitions by Electrons,* Vol. 88 of *Springer Tracts in Modern Physics* (Springer, Berlin, 1980).
[15]L. S. Caputi, E. Colavita, M. De Crescenzi, S. Modesti, L. Papagno, R. Scarmozzino, R. Rosei, and E. Tosatti, Solid State Commun. 39, 117 (1981).
[16]J. R. Rowe, G. Margaritondo, and S. B. Christman, Phys. Rev. B 15, 2195 (1977).
[17]G. A. Sawotzky, Phys. Rev. Lett. 39, 504 (1977).
[18]M. Cini, Solid State Commun. 24, 681 (1977).
[19]P. J. Feibelman, E. J. Mc Guire, and K. C. Pandey, Phys. Rev. B 15, 2202 (1977).
[20]L. E. Davis, N. C. McDonald, P. W. Palmerg, G. E. Riach, and R. E. Weber, *Handbook of Auger Electron Spectroscopy* (Physical Electronics Industries, Eden Prairie, 1976).
[21]P. Pianetta, Ph.D. thesis, Stanford University, Stanford, CA, 1976 (unpublished).
[22]C. M. Garner, I. Lindau, C. Y. Su, P. Pianetta, and W. E. Spicer, Phys. Rev. B 19, 3944 (1979).
[23]L. J. Brillson, C. F. Brucker, N. G. Stoffel, A. D. Katnani, and G. Margaritondo, Phys. Rev. Lett. 46, 838 (1981).
[24]J. M. Andrews and J. C. Phillips, Phys. Rev. Lett. 35, 56 (1975).
[25]L. J. Brillson, Phys. Rev. Lett. 40, 260 (1978).
[26]See, e.g., G. Le Lay, M. Manneville, and R. Kern, Surf. Sci. 72, 405 (1978); T. Hanawa and K. Oura, J. Appl. Phys. 16, 519 (1977).
[27]L. J. Brillson, Phys. Rev. Lett. 18, 245 (1977).
[28]E. A. Stern and R. A. Ferrell, Phys. Rev. 120, 130 (1960).
[29]J. W. Gadzuk, Phys. Rev. B 1, 1267 (1970).
[30]H. Ibach and J. E. Rowe, Phys. Rev. B 9, 1951 (1974).
[31]H. Hiraki and M. Iwami, Jpn. J. Appl. Phys. Suppl. 2 Pt. 2 (1974).
[32]E. Hauser, R. J. Zirke, J. Tauc, J. J. Hauser, and S. H. Nagel, Phys. Rev. Lett. 40, 1733 (1978).
[33]M. L. Thèye, Phys. Rev. B 2, 3060 (1970).
[34]N. E. Christiensen and B. O. Seraphin, Phys. Rev. B 4, 3321 (1971).
[35]O. Bisi, C. Calandra, I. Abbati, L. Baricovich, I. Lindau, and W. E. Spicer (unpublished).
[36]P. S. Ho, G. W. Rubloff, J. E. Lewis, V. L. Moruzzi, and A. R. Williams, Phys. Rev. B 22, 4784 (1980).
[37]J. D. Riley, L. Ley, J. Azoulay, and K. Tarakura, Phys. Rev. B 20, 776 (1979).
[38]G. Ottaviani, K. N. Tu, and J. W. Mayer, Phys. Rev. Lett. 44, 284 (1980).
[39]D. Beaglehole, M. De Crescenzi, M. L. Thèye, and G. Vuye, Phys. Rev. B 19, 6303 (1979).
[40]M. Hansen and K. Anderko, *Constitution of Binary Alloys* (McGraw-Hill, New York, 1958).
[41]R. M. Tromp, E. van Loenen, R. G. Smeenk, F. W. Saris, F. Nave, and G. Ottaviani, paper presented at European Conference on Sobol Surfaces (ECOSS 4), Munster, 1981.